

# EMISSION LINE—ULTRAVIOLET TO X-RAY CONTINUUM CORRELATIONS: CONSTRAINTS ON THE ANISOTROPY OF THE IONIZING CONTINUUM IN ACTIVE GALACTIC NUCLEI

TING-GUI WANG, YOU-JUN LU and YOU-YUAN ZHOU

Center for Astrophysics, University of Science and Technology of China, Hefei, Anhui 230026, P R  
China

## ABSTRACT

Anisotropic emission of the ionizing continuum is a general prediction of the accretion disk models. In this paper, we present the results of correlation analysis of the UV emission line and UV to X-ray continuum properties for a large sample of broad emission line AGNs observed with ROSAT, IUE and HST. We find strong correlations between the CIV/ $Ly\alpha$  ratio, the equivalent width of CIV, and the UV to soft X-ray spectral slope. The results are in good agreement with the photoionization calculation, suggesting that the overall ionizing continuum can well match the observed UV to soft X-ray spectrum. These results are consistent with the assumption of isotropic ionizing continuum shape. Our analysis suggests a small range for the “big blue bump” cutoff energy for the objects in this sample, consistent with the similar results of Laor et al. 1997, Walter & Fink 1993 based on the continuum properties. The mean UV-to-X-ray spectral slope is similar to the soft X-ray spectral slope. This similarity also holds for radio-loud and radio-quiet objects separately. This suggests that the two might be drawn from the same distribution. The two spectral slopes are only weakly correlated. The UV to X-ray spectral index is correlated with absolute optical magnitude. This result confirms the earlier suggestion that the ionizing continua are softer for higher luminosity objects.

*Subject headings:* galaxies: nuclei – quasars: general

## 1. INTRODUCTION

It is generally accepted that the enormous energy output of Active Galactic Nuclei is produced by the accretion of material onto putative super-massive black holes. The large angular momentum present in the interstellar medium suggests that the accreted gas is most likely to form an accretion disk, and a variety of evidences for axisymmetry supports this idea. The accretion disk can be of a geometrically thin, thick or intermediately slim form. The spectral energy distribution (SED) and the intensity of the radiation from such disks are expected to be highly anisotropic (e.g., Cunningham 1975, Laor, Netzer & Piran 1990, Madau 1988 ). This effect is particularly

important in the UV to X-ray band, which comes from the inner-most part of the accretion disk, where general relativistic effects are important. However, direct measurement of the anisotropy of radiation in a single object is impossible because we can only measure the radiation in a specific direction. An indirect measurement made using the very extended narrow emission line region suggests that the nuclear radiation is anisotropic (e.g., Wilson 1994). However, the anisotropy evidenced in this way is expected to originate at a much larger scale (e.g., by an obscured torus) rather than in the nuclear region.

Broad emission lines that cover a wide range of ionization levels are thought to be produced by photoionization. According to the photoionization theory, the lines from different ionization levels respond to different parts of the ionizing continuum. For example, Ly $\alpha$  is produced by photons with energy at  $\geq 13.6\text{eV}$ , CIV by photons with  $E \geq 48\text{eV}$ . Therefore the line spectrum provides a way of diagnosing the shape and intensity of the ionizing continuum. Since it is impossible to resolve the BLR spatially, only the total intensities of emission lines can be obtained. The observed line ratios and equivalent widths are dependent on some average shape and intensity of the ionizing continuum illuminating the BLR, which should be different from the observed one if the continuum emission is anisotropic. Therefore a comparison between the ionizing continuum required to reproduce the broad line spectrum and the observed continuum can constrain the role of anisotropy in the continuum emission.

For individual objects, such a comparison is very difficult to make. First, the emission line spectrum depends on the input ionizing continuum, on the physical parameters and on the chemical abundances of line emitting gas. Since there are no independent methods other than modeling the emission line spectrum to determine the physical conditions of line emitting gas, determination of the ionizing continuum from the emission line spectrum requires accurate measurements of emission lines of individual elements over a wide range of ionization, which is usually not possible. Second, the ionizing continuum at EUV energies is not directly observable because of interstellar absorptions.

However, a statistical study of this problem is feasible. The current photoionization model can explain reasonably well the average observed strong-UV lines (Netzer 1990); hence, the average physical parameters can be inferred in a statistical sense. Furthermore, a great number of UV and soft X-ray spectra have been accumulated with IUE, HST, and ROSAT in the past 5 yr (e.g., Wills et al. 1995, Zheng et al. 1997, Courvoisier & Paltani 1992, Brinkmann 1994). The ROSAT PSPC can detect the soft X-ray spectrum down to energy of 0.1 keV (Trümper 1983) for low redshift AGNs. For bright high redshift quasars at redshift  $z=4$ , the IUE and HST spectra can access emitted energies of up to 40 eV in the source rest frame. These observations make it possible to measure the emitted continuum up to energies of  $E \sim 10\text{--}40\text{eV}$ . If the intrinsic absorption is not significant (i.e., no strong absorption edges are seen), then the UV to X-ray spectrum can be roughly determined.

In this paper, we present a detailed study of the correlation between the broad emission

line spectrum and UV to X-ray continuum properties for a large sample of AGNs observed with ROSAT/PSPC and IUE, HST. The sample and techniques of data reduction are presented in §2. We present a statistical analysis in §3. Detail photoionization calculations are compared with the statistical results in §4, and the main conclusions are summarized in §5.

## 2. The Sample and Data Reduction

The heterogeneous sample consists of the 74 AGNs, the X-ray and UV spectra of which were analyzed for various purposes (Wang et al. 1996a, Wang et al. 1996b ), together with a number of AGNs observed by HST (Laor et al. 1994, Laor et al. 1995). The ROSAT spectra of 39 objects in this sample were taken from Wang, Brinkmann & Bergeron (1996a), and 3 from Brinkmann et al. (1995). The X-ray spectra for the remaining 32 objects were retrieved from ROSAT archive at Max-Planck-Institut für Extraterrestrische Physik and processed in the manner described below.

The UV spectra of 66 AGNs have been retrieved from IUE/ULDA (Uniform Low dispersion data archive), and were processed with IUE/SIPS. Average spectra have been made for those objects through multiple observations. A correction was made for Galactic reddening before any line or continuum parameters were measured. The Galactic reddening was estimated from the neutral hydrogen column value given by Dickey & Lockman (1990) with a conversion factor (Diplas & Savage 1994) of

$$E(B - V) = \frac{N_H^G}{5.51 \times 10^{21} \text{cm}^{-2}} \quad (1)$$

where  $N_H^G$  is the Galactic hydrogen column density. The values of  $E(B-V)$  are listed in Table 1. The uncertainty in  $N_H^G$  is about  $10^{20} \text{cm}^{-2}$ , corresponding to an uncertainty in  $E(B - V)$  of about 0.02. This introduces an uncertainty of  $\sim 20\%$  in the UV flux at  $1350\text{\AA}$ . Note the line ratio  $\text{CIV}/\text{Ly}\alpha$  is almost insensitive to the reddening correction for the sample used here. No attempt has been made to correct the intrinsic reddening, as it is rather uncertain. It is likely that the intrinsic reddening is small for our sample, since the soft X-ray fitting does not suggest significant absorptions above the Galactic columns (see below) for most objects.

The spectral indices in UV ( $\alpha_{UV}$ ) are determined by fitting a power-law function ( $f_\lambda \propto \lambda^{-2+\alpha_{UV}}$ ) to the dereddened UV spectra over several pseudo-line free windows, 1150-1180, 1335-1365, 1450-1480, 1760-1800 $\text{\AA}$  (in the source rest frame). The continuum flux at  $1350\text{\AA}$  has been determined by averaging the flux over the corresponding pass band, while the mean deviation is taken as uncertainty. The uncertainty given in this way is purely statistical and at the  $\sqrt{N} - 2\sigma = 2\sigma$  level (where  $N$ = width of the passband/IUE spectral resolution  $\simeq 6$  is the number of independent data points used for taking the average). The typical  $1\sigma$  level uncertainty for UV flux at  $1350\text{\AA}$  is about 10-20%. The emission line fluxes are measured by fitting the line profiles with multiple Gaussians. For strong lines, such as CIV and  $\text{Ly}\alpha$ , usually two Gaussians are used if the line profile is symmetric, and three Gaussians if it is asymmetric. For the S/N ratios of the spectra used here, three Gaussians are a good fit to the data. One Gaussian is used

for fitting the weak lines, such as NV, HeII, SiIV+OIV], where the line centers have been fixed at the observed wavelength. The fitting is done locally using the IRAF package. The fitted regions are 1180-1290, and 1480-1700Å for  $Ly\alpha$ +NV and CIV+HeII, respectively. They are subject to changes when there is contamination in the fitting region such as geo-coronal  $Ly\alpha$  for very low redshift AGN or when part of fitting region is shifted out of the spectral coverage. For the four objects, (3C351, PG1411+442, PG1351+640, NGC3516) with obvious associated UV line absorptions, the absorption troughs have been modeled with single Gaussian. The emission line flux is calculated by adding up all the emission line components. Because of the low S/N ratio of these data, the FWHM of the emission line is measured from the synthetic spectrum, which is constructed by putting all the individual Gaussian components together. The FWHM measured in this way is less affected by the noise or the presence of weak blemishes. These results are given in Table 1. As compared with the results of Wang et al. (1996b), the typical uncertainty due to the measurement for  $CIV/Ly\alpha$  is about 0.12.

We have also included eight objects observed by HST in our sample. Among these, 3C232 shows obvious absorptions in CIV and NV. The line and continuum parameters are simply taken from Laor et al. (1994,1995), who adopted a similar, but more precise model for emission lines, having better S/N ratio data but using a different method for estimating continuum flux. These lines and continuum fluxes have also been corrected for Galactic reddening.

The ROSAT PSPC spectra have been reduced using the EXSAS package (Zimmermann et al. 1994). The source counts were extracted from a circular region centered on the AGN with a radius of 3.2 arcmin. The background was estimated from an annular source-free region. The spectrum was corrected for vignetting and dead-time, and regrouped to at least 20 counts per bin. The spectrum was then fitted with a single power law with Galactic absorption  $N_{ph}(E) = A \exp(-\sigma_E N_H) E^{-\Gamma}$ , where  $\sigma_E$  is the photoelectric absorption cross-section (Morrison & McCammon 1983) and  $N_H$  is the absorption column density. For most objects in the sample, a reasonable fit can be obtained with the single power law description, and the  $N_H$  values are consistent with the Galactic  $N_H^G$  values in the corresponding direction (Dickey & Lockman 1990). Only 7 objects (III ZW 2, I ZW 1, PKS 0405-123, 3C 120, Mark 79, Q 1244+0240, 3C 390.3) in the sample show excessive absorptions larger than  $10^{20} \text{ cm}^{-2}$  and at greater than  $2\sigma$  significant level. The X-ray spectral index ( $\alpha_X$ ) is related to above photon index  $\Gamma$  by  $\alpha_X = \Gamma - 1$ . The results are presented in Table 2, where all error bars are quoted at  $1\sigma$  level. In Table 2, we also present the absolute bolometric magnitudes ( $M_{abs}$ ) of the sources, which are taken from Veron-Cetty & Veron (1996).

### 3. Statistical Analysis

From the data in Table 1 and Table 2, the UV to X-ray spectral slope is calculated using

$$\alpha_{UVX} = -0.491 \log(f_{1kev}/f_{1350}). \quad (2)$$

where,  $f_{1kev}$  and  $f_{1350}$  are flux at 1 keV and 1350Å respectively. As we have discussed in the last section, the typical uncertainty in the flux at 1350Å due to the measurement uncertainty plus the uncertainty in the Galactic reddening correction is estimated to be 40%. The typical uncertainty in the X-ray flux at 1 keV is 10%. Therefore a combination of these will introduce a typical uncertainty in  $\alpha_{UVX}$  of about 0.10.

We have also calculated the spectral slope ( $\alpha_{EUV}$ ) between the UV and the soft X-ray at 0.2 keV. The uncertainty for X-ray flux at 0.2 keV is considerably larger than the corresponding error at 1 keV because the 0.2 keV flux is very sensitive to the absorption correction. For example, if the  $N_H$  value varies by  $10^{19}cm^{-2}$ , the flux at 0.2 keV will change by 10%. An uncertainty of  $10^{20}cm^{-2}$  in the  $N_H$  means an uncertainty of 160% in the 0.2 keV flux, or an uncertainty 0.4 in the  $\alpha_{EUV}$

The distributions of  $\alpha_{UVX}$  and  $\alpha_X$  are plotted in Figure 1. The Kolmogorov-Smirnov test (Press et al. 1992) gives a probability of P=4%. Thus the two data sets are drawn from the same distribution. Since the uncertainty in  $\alpha_X$  is considerably larger than the uncertainty in  $\alpha_{UVX}$ , the Kolmogorov-Smirnov test may give a false indication because of variance introduced by different uncertainties in the data. To address this concern, we take only the objects with small uncertainties in  $\alpha_X$ . The Kolmogorov-Smirnov test gives a D=0.22, P=0.08 and D=0.18, P=0.32 for the subsample with  $\sigma(\alpha_X) < 0.5$  (N=69 objects) and  $\sigma_{\alpha_x} < 0.3$  (N=55), respectively. This result suggests that the different distribution indicated by the Kolmogorov-Smirnov test for the whole sample is due to the objects with large uncertainties in  $\alpha_X$ .

For this heterogeneous sample, the mean  $\langle \alpha_{UVX} \rangle = 1.49 \pm 0.03$  is in different from  $\langle \alpha_X \rangle = 1.46 \pm 0.05$ , where the error here and below is the uncertainty in the mean. This relation  $\langle \alpha_X \rangle \simeq \langle \alpha_{UVX} \rangle$  also holds when the sample is broken down into the radio-loud objects (17 radio galaxies and radio-loud quasars) where  $\langle \alpha_X \rangle = 1.38 \pm 0.14$  and  $\langle \alpha_{UVX} \rangle = 1.45 \pm 0.12$ , and to radio quiet objects where  $\langle \alpha_X \rangle = 1.48 \pm 0.10$  and  $\langle \alpha_{UVX} \rangle = 1.51 \pm 0.07$ . A similar result for  $\langle \alpha_{OX} \rangle \simeq \langle \alpha_X \rangle$  has been noted by Brunner et al. (1992), Turner, George & Mushotzky (1993) and Laor et al. (1997). We have also checked to see whether the two spectral indices have similar medians. The medians are 1.53 for  $\alpha_{UVX}$  and 1.39 for  $\alpha_X$ . If the uncertainty were normally distributed, the median would not be sensitive to the uncertainty. However, the error distribution in  $\alpha_X$  is very likely asymmetrical, therefore the small difference in the median could be due to the larger uncertainty in the  $\alpha_X$ . Subsequent analysis confirms this. When a subsample of objects with uncertainty in  $\alpha_X$  less than 0.2 (41 objects) is considered, the medians for  $\alpha_{UVX}$  and  $\alpha_X$  are 1.50 and 1.48, respectively. These analyses suggest that  $\alpha_X$  and  $\alpha_{UVX}$  might be drawn from the same distribution.

Although Laor et al. (1997) claimed that the distribution of  $\alpha_{OX}$  is bimodal based on their sample of 23 objects and on the Figure 5b of Wang et al. (1996b), we did not find similar result for  $\alpha_{UVX}$  in our sample.

Spearman rank correlation analysis has been performed among four continuum parameters:

$\alpha_X$ ,  $\alpha_{UVX}$ ,  $\alpha_{UV}$ , and the absolute Magnitude  $M_{abs}$ ; and among five emission line parameters: Equivalent widths (EWs) and FWHM of CIV and  $Ly\alpha$  and the line ratio CIV/ $Ly\alpha$ . The correlation matrix is presented in Table 3. Among 36 pair of combination, we found correlation caused by random factors with a probability less than 1% for 24 pairs. Some correlations are obvious, such as between  $\alpha_{UV}$  and  $\alpha_{EUV}$ , and between the FWHM of CIV and the FWHM of  $Ly\alpha$ . Some others have been discovered previously, such as the anti-correlations between  $M_{abs}$  and EW(CIV), known as the Baldwin effect, and between  $M_{abs}$  and line ratio CIV/ $Ly\alpha$ , the positive correlations between the EWs of CIV or  $Ly\alpha$  and the emission line width of CIV or  $Ly\alpha$  (Wills et al. 1993); and the correlation between the line ratio CIV/ $Ly\alpha$  and the line width of CIV or  $Ly\alpha$ . We will not discuss these correlations because they have been extensively discussed in the literature (e.g., Wills et al. 1993; Wang et al. 1996a).

### 3.1. Correlations among continuum properties

The UV-to-X-ray spectral slope ( $\alpha_{UVX}$ ) is correlated with absolute magnitude with a correlation coefficient  $R_s = -0.50$  corresponding to a probability caused by a random factor of  $P_r = 5 \times 10^{-6}$ . Similarly, the  $\alpha_{EUV}$  is also correlated with  $M_{abs}$  with  $R_s = -0.50$  and  $P_r = 5 \times 10^{-6}$ . These correlations are similar to those between  $\alpha_{OX}$  and luminosity (e.g., Yuan et al. 1997), indicating that the ionizing spectrum is softer when the luminosity is higher. However, neither the soft X-ray nor the UV spectral index is correlated with absolute magnitude. The  $\alpha_{UVX}$  is weakly correlated with  $\alpha_X$  (figure 2). The correlation for our heterogeneous sample is substantially weaker than the one found in a sample of 58 bright Seyfert galaxies (Walter & Fink 1993). The correlation coefficient is only 0.44, corresponding to  $P_r = 2 \times 10^{-4}$ . Fitting the data points to a straight line (Press et al. 1992) yields  $\alpha_X = (0.61 \pm 0.04) + (0.60 \pm 0.09)\alpha_{UVX}$  with a  $\chi^2 = 170.5$  for 74 data points, which is accepted at a probability of only  $Pr = 6 \times 10^{-10}$ . We have taken into account both errors in the  $\alpha_X$  (Press et al. 1992), with a typical error of 0.5 assigned for objects with no error presented in Table 2, and in the  $\alpha_{UVX}$ , for which a typical uncertainty of 0.1 is assigned.

### 3.2. Correlation between line and continuum properties

The CIV/ $Ly\alpha$  ratio is strongly correlated with  $\alpha_{UVX}$  with  $R_s = -0.58$  (see figure 3), in the sense that a flat UV to-X-ray spectrum corresponds to a larger CIV/ $Ly\alpha$ . This correlation is not affected by whether or not the four objects with associated absorption lines, PG1411+442, PG1351+640, 3C232 and 3C351 (the redshift of NGC3516 is too low to have  $Ly\alpha$  reliably measured), are included. The UV to-X-ray spectra of these four absorbed objects are very steep. We have also noted that the other AGN with  $\alpha_{UVX} > 2.0$ , PG0844+349 also shows an UV CIV absorption line in the HST FOS spectrum (Corbin & Boroson 1996). Furthermore, the radio-loud (RL) and radio-quiet (RQ) objects show no difference on the plot. This is consistent with the

general indifference in the average CIV/Ly $\alpha$  ratio between RQ and RL QSOs (e.g., Wilkes 1986). IZW 1, Mrk478, and PG1012+008 show significantly low CIV/Ly $\alpha$  as compared with other objects with similar  $\alpha_{UVX}$ . Actually, their UV to X spectral slopes are quite normal, while their CIV/Ly $\alpha$  ratios for these three are the lowest. Mrk478 and I ZW 1 are typical narrow line Seyfert 1 galaxies with strong optical FeII emission (Boroson & Green 1992); it has already noted by Wang et al. (1996b) that strong optical FeII emitters tend to have weak CIV emission. However, the optical spectrum of PG1012+008 is quite normal. The low CIV/Ly $\alpha$  ratio cannot be due to measurement error. The CIV line in the spectrum of PG1012+008 as processed with the method of optimal extraction also appears extremely weak on the plot of Lanzetta, Turnshek, & Sandoval (1993). A correlation between the CIV/Ly $\alpha$  ratio and the soft X-ray spectral slope is also found, with  $R_s = -0.43$ , corresponding to  $P_r = 1 \times 10^{-4}$ .

The EW of CIV is much better correlated with  $\alpha_{UVX}$  ( $R_s = -0.59$ ,  $P_r = 3 \times 10^{-8}$ ) than the Ly $\alpha$  EW ( $R_s = -0.43$ ,  $P_r = 2 \times 10^{-4}$ ) (figure 4) is. The CIV EW appears to be also correlated with  $\alpha_X$  ( $R_s = -0.46$ ,  $P_r = 5 \times 10^{-5}$ ) and Ly $\alpha$  EW appears to be correlated with  $\alpha_{UV}$  ( $R_s = -0.38$ ,  $P_r = 0.001$ ).

The correlations of line parameters with  $\alpha_{EUV}$  are similar to those with  $\alpha_{UVX}$  (see Table 3). The slightly lower correlation coefficients are probably due to the larger uncertainties in the 0.2keV flux caused by the uncertainty in the absorption correction.

#### 4. DISCUSSION

We have found strong correlations between the CIV/Ly $\alpha$  ratio, the CIV EW, and the observed UV to X-ray continuum shape for a large sample of AGNs observed by ROSAT/PSPC and IUE, HST. These correlations have also been noted for a small sample of AGNs (Schulz 1992, Green 1996). Similar correlations between the OVI/Ly $\alpha$  ratio, OVI EW, and the UV to X-ray spectral slope have been reported by Zheng et al. (1995) for a small sample of moderate-redshift AGN observed by IUE, the Hopkins Ultraviolet Telescope (HUT) and HST. In this section we will discuss the implications of these results.

The predicted emission-line spectrum is sensitive to the exact shape of the “blue bump” in the UV to soft X-ray, since it is the photons at these energies that govern the ionization level and the excitation of the most commonly observed emission lines (e.g., Binette et al. 1989). In addition, Ferland et al. (1992) showed that the spectral shape at 0.1-1mm can also alter the strength of collisional-excited line CIV. That the observed CIV/Ly $\alpha$  decreases with increasing steepness of the ionizing continuum shape in UV to X-ray is in qualitative agreement with expectation of photoionization models. One obvious suggestion is that the observed continuum shape is related to average ionizing continuum of BLR. In the worst case, i.e., we assume that all the dispersions in the relation are due to intrinsic continuum anisotropy (see Fig. 4), and thus the maximum anisotropy produces a scatter in  $\alpha_{UVX} \simeq 1$ . However, the actual situation is much better than

this (see below).

In order to see how the observed data match the photoionization prediction, we have made a series of photoionization calculations using Cloudy 84.12 (Ferland 1994). We have assumed solar abundances, because CIV is the main coolant in the ionized hydrogen (HII) zone and because CIV emission is mainly determined by the heating rate at that zone; therefore the CIV/ $Ly\alpha$  ratio is not very sensitive to the assumed chemical abundances (Davidson & Netzer 1979). The hydrogen column density is assumed to be  $10^{23} \text{ cm}^{-2}$ . Other values should produce similar CIV/ $Ly\alpha$ , provided the gas is not too optically thin. The ionization parameter (the ratio of the ionizing photon density and particle density) and particle density range from  $10^{-2.5}$  to 0.1 and from  $10^9$  to  $10^{10} \text{ cm}^{-3}$ , respectively. The input ionizing continuum is approximated by a power law between the far UV and 1 keV with varying spectral slope, similar to the composite EUV spectrum found by Zheng et al. (1997) for a sample of quasars observed by HST, but otherwise similar to the “mean AGN spectrum” of Mathews & Ferland (1987). In addition, the geometry of broad emission line cloud distribution is assumed to be spherical, so the line intensity is the average of the emission from the illuminated and the back surfaces of the clouds. If the distribution of broad line clouds were not symmetrical geometry, then the line emission would be anisotropic, and the observed line ratios would depend on the inclination. For optically thick clouds, the  $Ly\alpha$  photons are more forward beamed than CIV photons are (Ferland et al. 1992). Consequently, the line ratio CIV/ $Ly\alpha$  is larger when one looks at the illuminated face, and smaller at the back face. Nevertheless, as long as some rotational symmetry is kept for the geometry and as long as there are no preferred absorptions on either the far or the near side of the clouds, the line ratios are similar for the spherical symmetric geometry (e.g., Kallman & Krolik 1986). The calculated CIV/ $Ly\alpha$  are plotted against  $\alpha_{UVX}$  in figure 3.

Obviously, the observed CIV/ $Ly\alpha$  versus  $\alpha_{UVX}$  can be reproduced with a relatively narrow range of physical parameters. The result shows that CIV/ $Ly\alpha$  ratio is much more sensitive to the physical conditions when the UV to X spectrum is harder. This is in good agreement with interpretation of the scatter in terms of different physical parameters. For  $n_H = 10^{10} \text{ cm}^{-3}$ , the range in U is about a factor of 20. This range is consistent with the results of reverberation mapping of bright AGNs for which the BLR size deviates from  $R \propto L^{1/2}$  by a factor of sometimes greater than 5 (e.g., Peterson 1993, Kaspi 1997). Therefore, this interpretation is sensible. And if the typical measurement error for CIV/ $Ly\alpha \sim 0.12$  is taken into account, the incident ionizing continuum on BLR must be very close to what we see. The UV to X-ray spectrum is likely not a power law, but a combination of “blue bump” and a hard power-law component. A different cutoff energy of the “bump” will further introduce scatter in the correlation (see below). A more detailed analysis requires higher quality data.

The correlation between the  $Ly\alpha$  EW and the  $\alpha_{UV}$  is a natural prediction if the observed UV spectrum extends to the Lyman limit and the BLR sees the same continuum as we do. However, the correlation between the  $Ly\alpha$  EW and  $\alpha_{UVX}$  requires that continuum slope in the Lyman continuum range also be related to the  $\alpha_{UVX}$  since  $Ly\alpha$  is produced mainly by recombination



process. Since  $\alpha_{UVX}$  is not correlated with  $\alpha_{UV}$  (see §3), this requires that the UV continuum extend to the Lyman limit to produce the former correlation, but not to too high energy, or it would destroy the latter. The fact that  $\alpha_{UV}$  is not correlated with CIV EW also suggests that the UV spectrum does not extend too far to the  $Ly\alpha$  limit continuum.

For the description of the “big blue bump” as  $f_\nu \propto \nu^{-\alpha_{UV}} e^{-h\nu/E_{cut}}$ , it is shown that the range in the cutoff energy,  $E_{cut}$ , is small (Walter & Fink 1993, Laor et al. 1997). With this range of  $E_{cut}$ , the CIV ionizing photon numbers do not change much; however, the heating rate changes significantly if the  $\alpha_{UVX}$  is soft. As a result, the CIV/ $Ly\alpha$  ratio is sensitive to the cutoff energy of the “big blue bump” (cf., Binette et al. 1989). Grid photoionization calculations are made for  $n_H = 10^{10} \text{ cm}^{-3}$ ,  $N_c = 10^{23} \text{ cm}^{-2}$ , and solar chemical abundance, with results in agreement with the above qualitative analysis (see figure 5). For example, for  $\alpha_{UVX} \sim 1.5 - 2.0$ , the difference in CIV/ $Ly\alpha$  ratio is 0.28 if  $E_{cut}$  vary from 30eV to 60 eV, which is similar to the value of the observed scatter in CIV/ $Ly\alpha$  versus  $\alpha_{UVX}$  correlation. A larger cut-off energy range would produce a scatter larger than the one observed. This analysis provides an independent evidence for a small range of cut-off energy.

Francis (1993) and Netzer, Laor & Gondhalekhar (1992) found that the distributions of CIV and  $Ly\alpha$  EWs are narrower than those expected for an ionizing continuum source from a randomly inclined accretion disk. Here, we show that the observed  $\alpha_{UVX}$  distribution can contribute a similar size to the scatter of  $Ly\alpha$  and CIV EWs. Taking away the  $\alpha_{UVX}$  factor, the distribution for  $Ly\alpha$  EW is narrowed down significantly. If one accepts the rough isotropy of UV to X-ray spectrum we argued above, the random thin disk distribution of ionizing continuum strength is even more problematic.

## 5. Conclusion

We have presented the results of correlation analysis of UV and soft X-ray spectra for a large sample of AGN. The main results are summarized as follows:

1. The UV-to-X-ray spectral indices are strongly correlated with line ratios CIV/ $Ly\alpha$ . This correlation can be modeled with photoionization models that assume ionizing continua with a range of UV to X-ray spectral slopes, and the scatter can be interpreted as due to the uncertainties in the physical conditions of the BLR. We suggest that the average ionizing spectrum striking the BLR is similar to the observed one. If the ionizing continuum consists of a power law and the “big blue bump” components, the range of bump cutoff energy must be small in order to be consistent with the correlation.
2. The UV to X-ray spectral indices are significantly correlated with the EWs of CIV and  $Ly\alpha$ . These correlations are also consistent with the the interpretation of isotropic ionizing continuum shape. As a consequence of this correlation, the constraints put by Netzer et al.

(1992) and Francis (1993) on the anisotropy of the continuum would be even stronger.

3. The UV to X-ray spectral index is correlated with absolute optical magnitude. This result confirms the earlier suggestion that the ionizing continua are softer for objects with higher luminosities.
4. The mean UV to X-ray spectral slope is similar to the soft X-ray spectral slope. This similarity also holds for radio-loud and radio-quiet objects separately. This suggests that the two may be drawn from the same distribution. The two spectral slopes are only weakly correlated.

We thank the anonymous referee for many useful suggestions that significantly improved the presentation of this paper. This work is partly supported by the Chinese Natural Science Foundation and the Pandan Project.

## REFERENCES

- Binette, L., Prieto A., Szuszkiewicz, E. & Zheng W. 1989, ApJ,343,135
- Boroson, T.A. & Green, R.F., 1992, ApJS, 80, 109
- Brinkmann, W., 1994, in IAU Symp. 159, Multi-Wavelength Continuum Emission of AGN, ed. T.J.L. Courvoisier & A. Blecha (Dordrecht: Kluwer), 53
- Brinkmann, W., et al. 1995, A&AS, 106, 303
- Brunner, H., Friedrich, P., Zimmermann H.U. & Stauhart R., 1992, in X-ray Emission from Active Galactic Nuclei and the Cosmic X-ray Background, ed. W. Brinkmann & J. Trümper, (MPI:Garching), 198
- Corbin, M.R. & Boroson, T.A., 1996, ApJS, 107, 69
- Courvoisier, T.J.-L & Paltani S.,1992, IUE-ULDA Access Guide No. 4, ESA Publications Division, ESTEC, Noordwijk, Netherland
- Cunningham, C.T., 1975, ApJ, 202, 788
- Davidson, K. & Netzer, H., 1979, Rev. Mod. Phys., 51, 715
- Dickey, J.H. & Lockman F.J., 1990, ARA&A, 28, 215
- Diplas, A., & Savage, B.D., 1994, ApJ, 427, 274
- Ferland, G.J., 1994, HAZY a brief introduction to CLOUDY 84, University of Kentucky Department of Physics and Astronomy Internal Report.
- Ferland, G.J., Peterson, B.M., Horne, K., Welsh W.F., & Nahar S.N. 1992, ApJ, 387, 95
- Francis, P.J., 1993, ApJ, 405, 119
- Green, P.J., 1996, ApJ, 467,61
- Kallman, T. & Krolik, J., 1986, ApJ, 308, 805
- Kaspi, 1997, in Emission Lines in Active Galaxies: New Methods and Techniques, ed. B.M., Peterson, F.Z. Cheng & A.S. Wilson (San Francisco: Astronomical Society of the Pacific), in press
- Lanzetta, K.M., Turnshek, A. & Sandoval, J. 1993 ApJ, 84, 109
- Laor, A., Netzer, H., & Piran, T., 1990, MNRAS242, 560
- Laor A., Fiore F., Elvis M., Wilkes B.J., & McDowell J.L., 1997, ApJ, 477, 93

- Laor A., Bahcall, J.N., Jannuzi B.J., Schneider, D.P., Green, R.F. & Hartig G.F. 1994, ApJ, 420, 110
- Laor A., Bahcall J.N., Jannuzi B.T., Schneider D.P. & Green R.F., 1995, ApJS, 99,1
- Madau, P., 1988, ApJ, 327, 116
- Mathews, W.G. & Ferland, G.J., 1987, ApJ323, 456
- Morrison R., McCammon D., 1983, ApJ, 270, 119
- Netzer, H., 1990, in "Physics of Active Galactic Nuclei", ed. R.D. Blandford, H. Netzer & Woltjer, p153
- Netzer, H., Laor, A. & Gondhalekhar P.M., 1992, MNRAS, 254, 15
- Peterson, B.M., 1993, PASP, 105, 247
- Press, W.H., Teukolsky, S.A., Vetterling, W.T. & Flannery, B.P., 1992, Numerical Recipes in C, Cambridge University Press, Cambridge.
- Schulz, H. 1992, in Physics of Active Galactic Nuclei, ed. W.J. Duschl & S. J. Wagner (Berlin:Springer), 235
- Trümper, J. 1983, Adv. Space Res., 4, 241
- Turner, T.J., George, I.M. & Mushotzky R.F., 1993, ApJ, 412, 72
- Walter, R. & Fink, H.H., 1993, A&A, 274, 105
- Wang, T., Zhou, Y. & Gao, A., 1996, ApJ, 457, 111
- Wang, T., Brinkmann, W. & Bergeron J., 1996, A&A, 309,81
- Wilkes, B.J., 1986, MNRAS, 218, 331
- Wills, B.J., Fang, D., Steidel, C.S., Sargent, W.L.W., 1993, ApJ,451,563
- Wills, B.J., et al., 1995, ApJ, 447, 139
- Wilson, A.S. 1994, in Proceedings of the Oxford Torus Workshop, ed. M.J. Ward, (Oxford University: Oxford UK), P. 55
- Yuan, W., Brinkmann, W., Siebert, J. & Voges, W. 1997, A&A, in press
- Zheng, W., Kriss, G.A. & Davidsen A.F., 1995, ApJ, 440, 606
- Zheng, W., Kriss, G.A., Telfer, R., Grimes, J., Davidsen, A., 1997, ApJ, 475,469
- Zimmermann, H.U., et al. 1994, EXSAS User's Guide, MPE-Report 257, (MPE:Garching)



Fig. 1.— The distributions of UV-to-X-ray spectral slope and the soft X-ray spectral slope. The solid line is for the  $\alpha_X$ , whereas the dashed line for  $\alpha_{UVX}$ . Typical sizes of error bar are 0.2 and 0.5 for  $\alpha_{EUV}$  and  $\alpha_X$ , respectively.

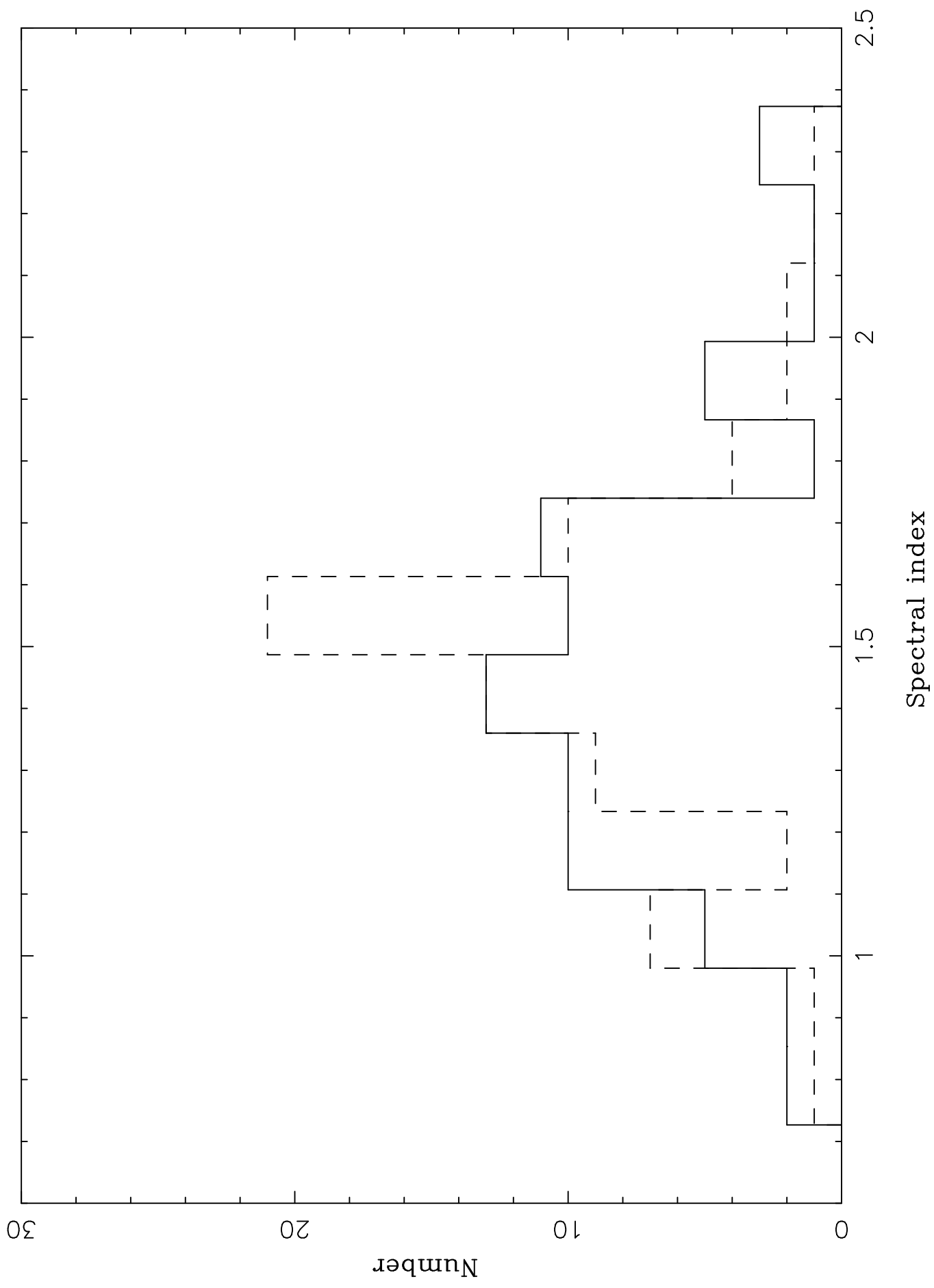
Fig. 2.— The ROSAT PSPC spectral indices  $\alpha_X$  versus the UV-to-X-ray spectral index ( $\alpha_{UVX}$ ). For the data from ROSAT All Sky Survey, the error bars for X-ray spectral index are not shown. The dashed line in the figure is  $\alpha_X = \alpha_{UVX}$ .

Fig. 3.— The correlation of line ratio CIV/Ly $\alpha$  versus UV-to-X-ray spectral index. Filled squares are for radio quiet objects, open circles are for the radio-loud objects. The theoretical predictions are shown as curves for hydrogen particle densities  $10^{10} \text{ cm}^{-3}$  (solid line) and  $10^9 \text{ cm}^{-3}$  (dashed-line). For each curve, the ionization parameters are labeled. Typical error bar is shown in the upper-right corner.

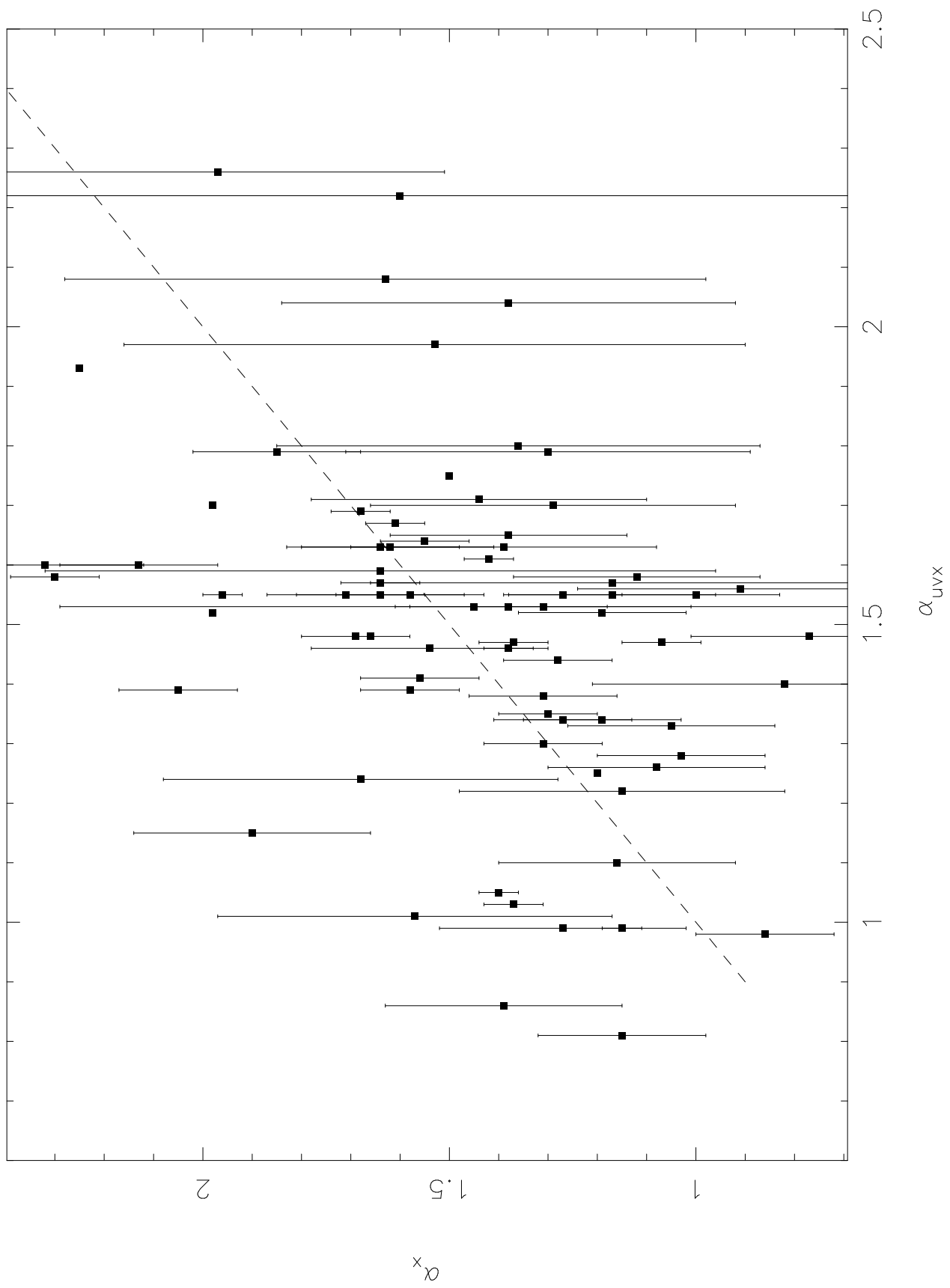
Fig. 4.— Correlations of line equivalent width with  $\alpha_{UVX}$ . The  $\alpha_{UVX}$  versus EW CIV correlation is stronger than the  $\alpha_{UVX}$  versus EW Ly $\alpha$  correlation is.

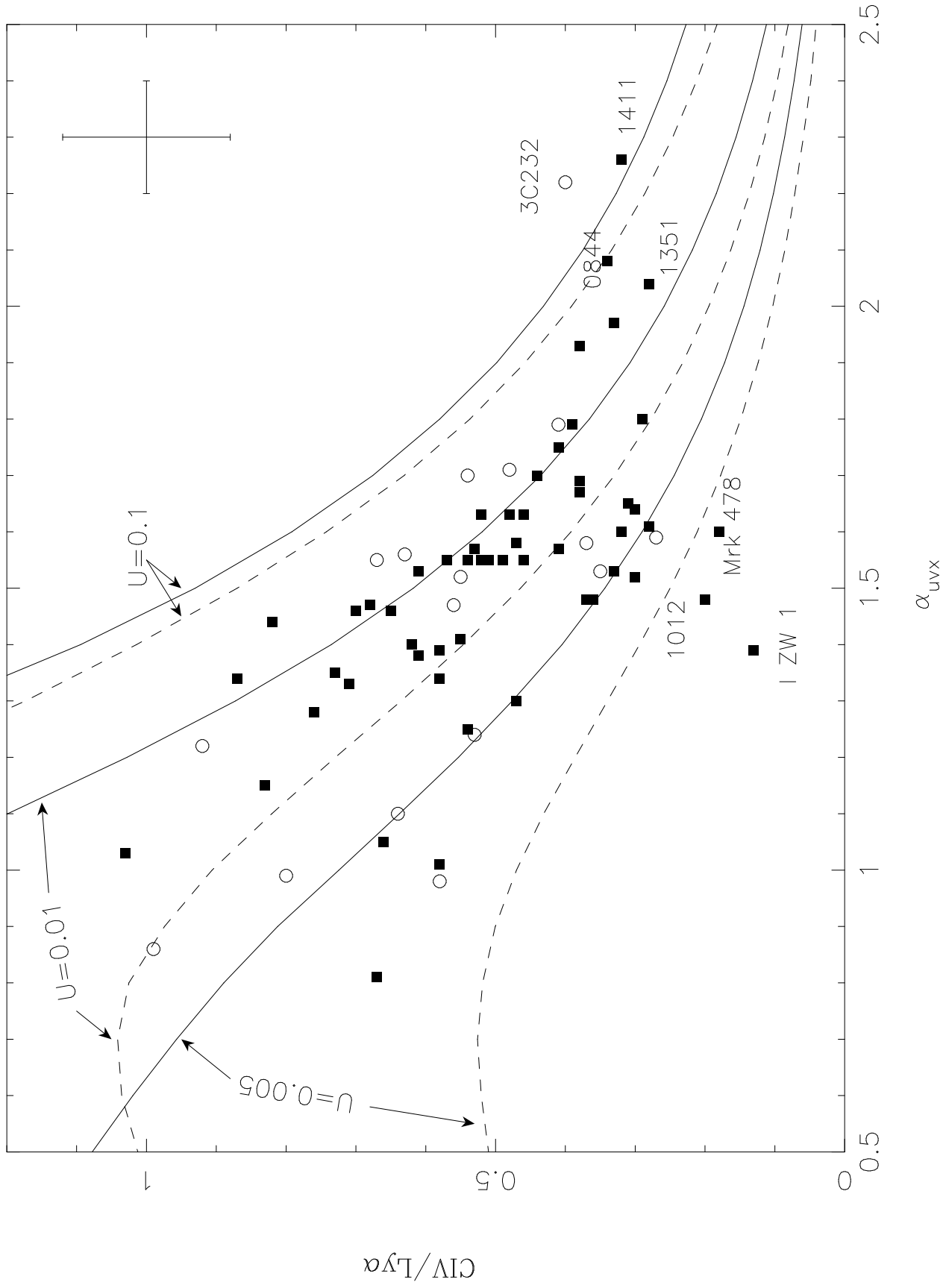
Fig. 5.— Illustration of the impact of cutoff energy of the “big blue bump” on the line ratio CIV/Ly $\alpha$  for various UV-to-X-ray spectral indices. The models adopted here use ionization parameter,  $U=0.01$ , column density  $N_H = 10^{23} \text{ cm}^{-2}$  and particle density  $n_H = 10^{10} \text{ cm}^{-3}$ .

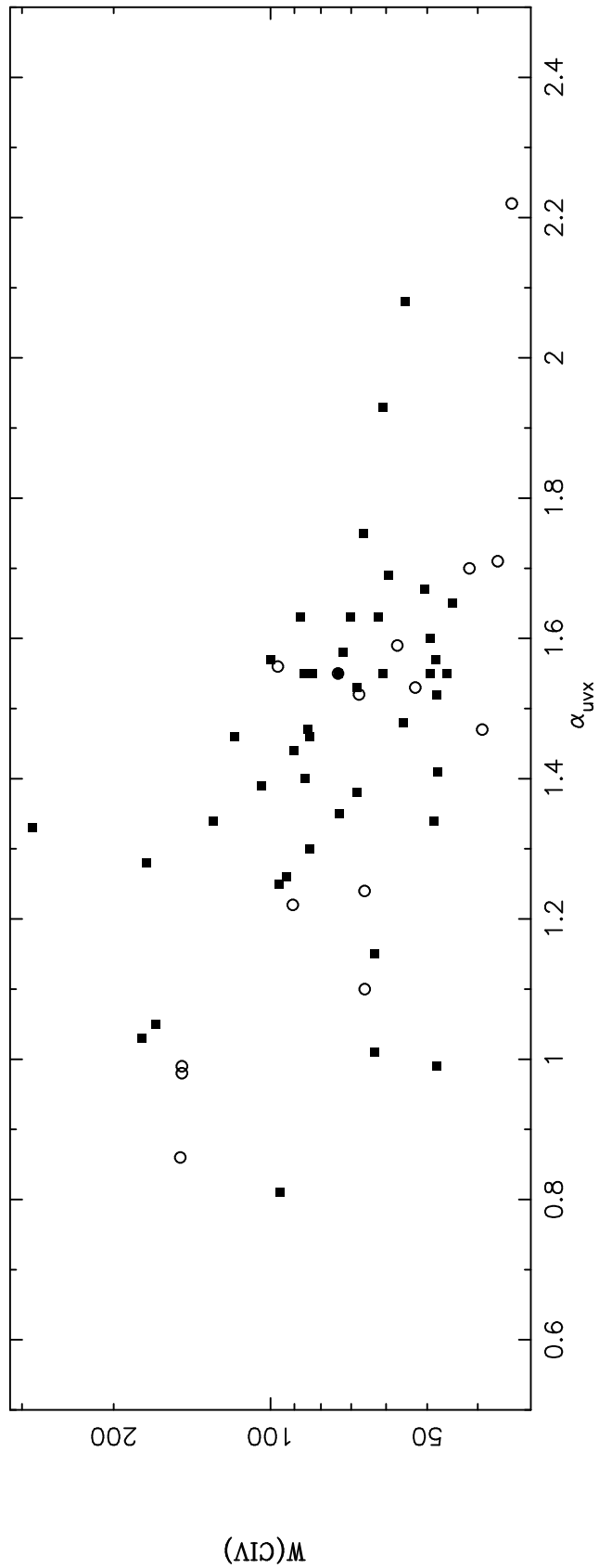
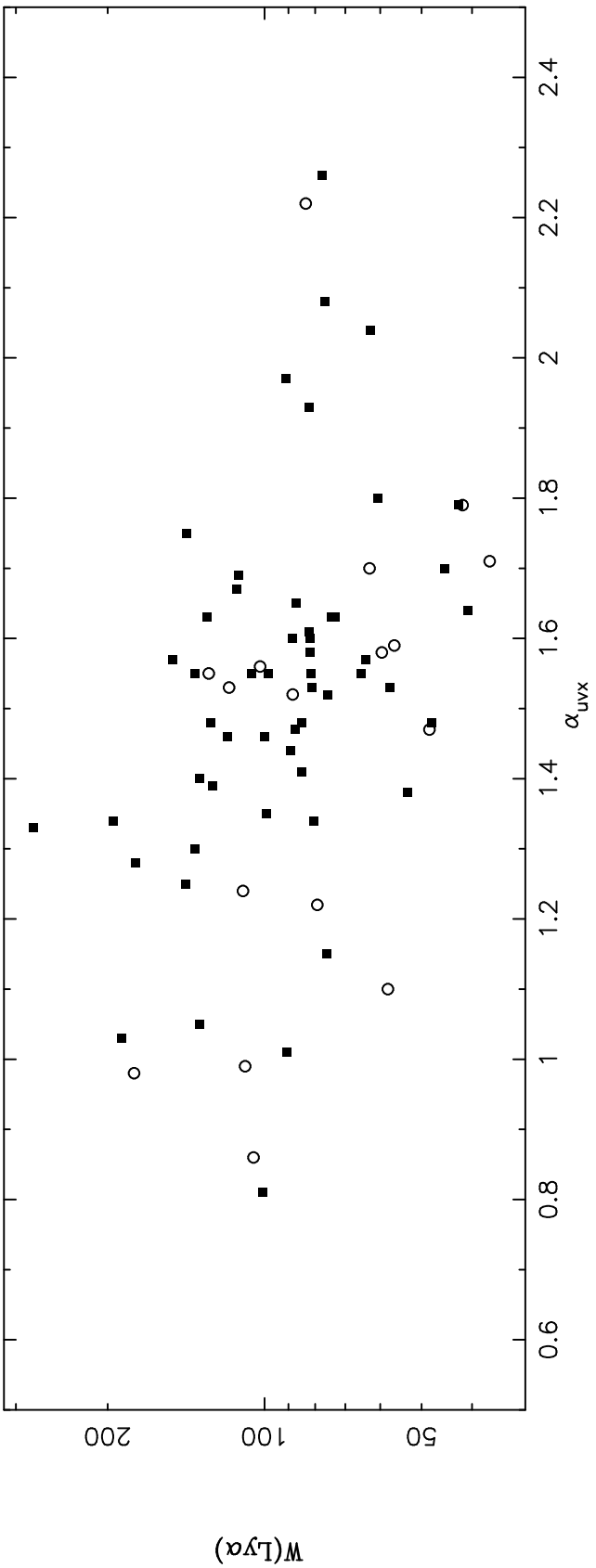












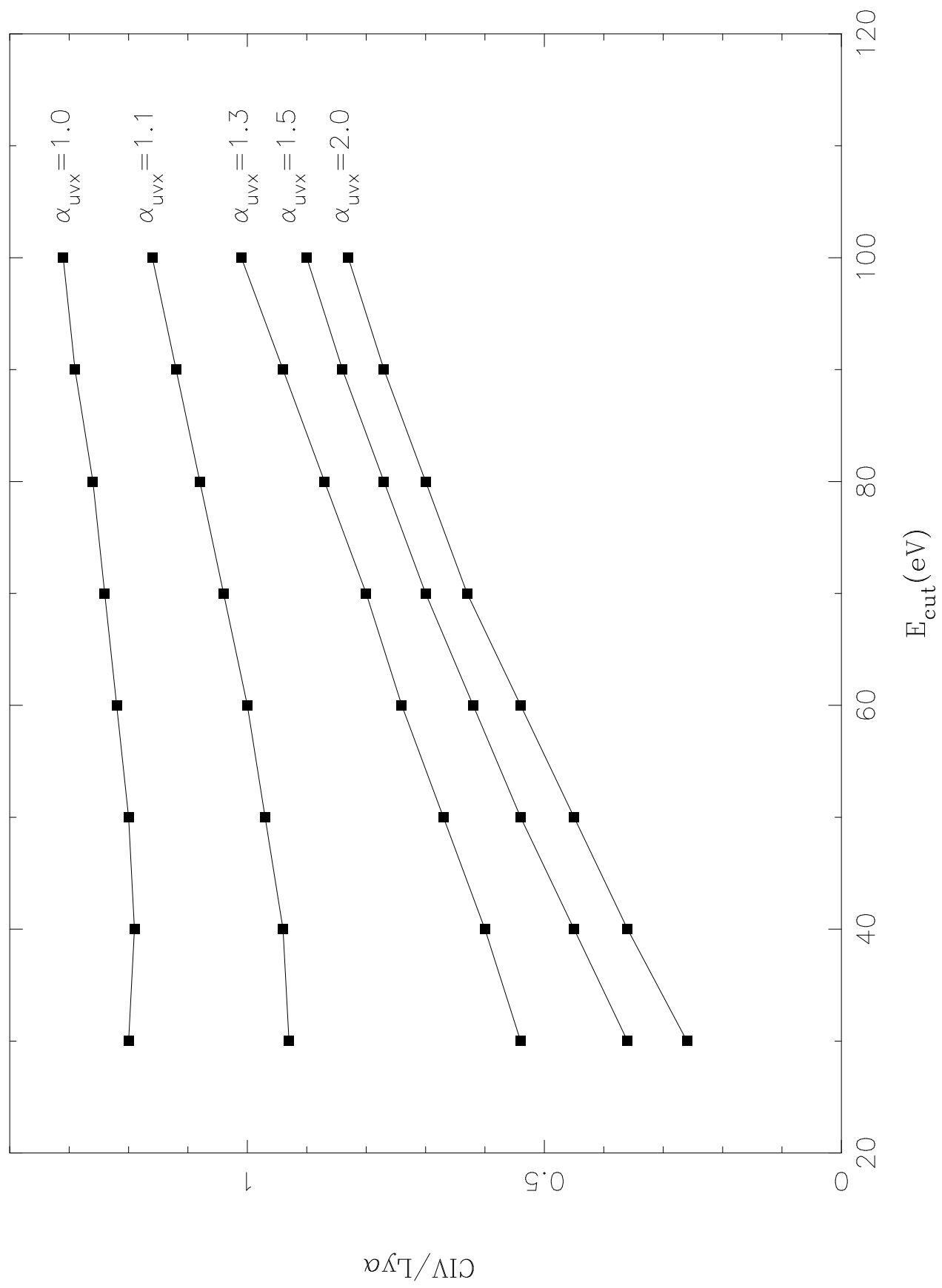


TABLE 1  
UV EMISSION LINE AND CONTINUUM PARAMETERS

Object	Other Name	E(B-V)	I <sup>a</sup> Ly $\alpha$	EW Ly $\alpha$	I <sup>a</sup> CIV	EW CIV	$\frac{CIV}{Ly\alpha}$	1350Å $\nu f_{\nu}$ <sup>b</sup>	$\alpha_{uv}$	FWHM <sup>c</sup> Ly $\alpha$	FWHM <sup>c</sup> CIV
0003+1955	MARK335	0.08	11.9	99	6.21	61	0.52	14.5±0.9	0.60±0.02	3691	3777
0007+1041	III ZW 2	0.11	3.33	128	2.23	74	0.67	3.75±0.63	1.24±0.04	4155	5120
0026+1259	PG	0.09	1.80	58	0.59	20	0.33	3.81±0.85	1.40 ± 0.14	3668	3788
0050+1225	I ZW 1	0.10	3.61	126	0.46	17	0.13	3.52±0.51	1.91±0.05	3364	2571
0052+2509	PG	0.09	5.02	106	2.72	83	0.54	4.87±1.35	0.12±0.14	5087	6653
0119-2836	TON S210	0.166	3.97	85	1.48	56	0.37	4.29±0.55	0.59±0.04	3853	5091
0121-5903	F 9	0.06	30.8	82	8.76	26	0.28	32.0±1.9	0.46±0.03	3740	4630
0124+1855	MARK359	0.09	2.33	53	1.41	68	0.61	3.27±0.33	0.63±0.06	1951	2000
0157+0009	MARK1014	0.05	1.26	42	0.49	30	0.39	2.68±0.48	0.43±0.07	3873	4184
0203-0031	MARK1018	0.05	2.11	82	0.99	72	0.47	1.97±0.42	0.73±0.15	3846	4847
0205+0228	NAB	0.07	1.68	60	0.62	18	0.37	2.82±0.68	1.08±0.08	2566	2708
0232-0900	NGC985	0.06	4.21	110	2.25	66	0.53	5.26±0.47	0.76±0.04	6456	6765
0236-5224	ESO198-G24	0.06	1.14	188	1.17	177	1.03	1.75±0.52	2.31±0.10	4241	6686
0405-123 <sup>1</sup>	PKS	0.03	2.59	88	1.42	67	0.55	3.33 ± ...	0.78±0.04	2282	3027
0430+0514	3C120	0.21	5.18	79	4.78	91	0.92	7.40±0.48	0.86±0.09	3595	3809
0513-0012	AKN120	0.22	34.0	113	13.0	51	0.38	33.6±1.1	0.91±0.02	6384	5710
0637-752	PKS	0.19	2.49	117	0.87	53	0.35	2.63±0.73	0.91±0.32	2515	2569
0702+6440	VII ZW 118	0.10	5.49	87	1.70	45	0.31	6.06±1.33	0.72±0.08	3157	4465
0738+4945	MARK79	0.11	5.19	76	4.29	63	0.83	8.24±0.65	0.34±0.06	4469	5552
0743+6103	MARK10	0.09	2.50	136	1.17	84	0.47	2.45±0.99	1.27±0.10	4694	4506
0804+7611	PG	0.06	5.26	82	2.58	49	0.49	8.01±0.66	0.44±0.03	5304	4444
0844+3456	PG	0.06	3.79	77	1.29	55	0.34	5.01±0.69	1.12±0.03	3466	4587
0915+1630	MARK704	0.07	1.46	91	0.84	63	0.57	1.81±0.43	1.88±0.07	3513	3759
0921+5230	MARK110	0.03	4.02	133	2.66	166	0.66	2.28±0.92	1.25±0.08	4585	3782
0923+129	MARK705	0.07	2.73	80	2.37	49	0.87	3.54±1.14	1.25±0.24	3680	4103
0953+415 <sup>1</sup>	PG	0.00	2.33	136	1.18	86	0.51	2.06 ± ...	0.76±0.10	2636	3067
0955+326 <sup>2</sup>	3C232	0.03	4.30	83	1.70	34	0.39	4.82 ± ...	1.48±0.05	2187	5526
1012+008	PG	0.07	1.17	127	0.23	31	0.20	1.20±0.42	0.50±0.41	4654	5933
1028+3118	B2	0.04	1.01	63	0.55	42	0.55	1.77±0.46	0.61±0.10	3661	4216
1100+772	3C249.1	0.07	2.27	56	0.62	57	0.27	2.81±0.61	-0.58±0.10	7298	9556
1103+7250	NGC3516	0.07	...	...	2.82	48	...	2.35±0.28	1.99±0.14	2738	3391
1114+445	PG	0.03	0.51	61	0.15	24	0.29	1.44±1.70	1.66±0.36	5547	2246
1116+2135 <sup>2</sup>	PG	0.02	6.24	112	2.40	59	0.38	5.45 ± ...	0.83±0.11	4220	4495
1119+1200	MARK734	0.05	2.60	76	0.78	48	0.30	2.79±0.44	0.39±0.12	2685	5425
1202+2810	GQ COM	0.03	0.97	89	0.80	90	0.82	1.18±0.34	0.45±0.18	4497	4921
1211+1419	PG	0.05	6.63	88	2.11	49	0.32	8.08±1.01	1.23±0.15	3051	3228
1216+069 <sup>2</sup>	PG	0.03	1.87	118	1.30	117	0.70	1.38 ± ...	0.82±0.07	2506	3039
1226+0219 <sup>1</sup>	3C273	0.00	13.6	48	7.58	39	0.56	32.1 ± ...	0.56±0.03	3101	3760
1229+2026	TON1542	0.04	3.66	64	1.50	48	0.41	5.34±0.49	0.24±0.03	3489	4904
1237-0504	NGC4593	0.04	...	...	1.90	93	...	2.24±0.22	1.90±0.03	5183	3660
1244+0240	Q	0.03	0.50	48	0.18	27	0.36	1.18 ± 34	1.40±0.13	2210	2531
1307+0835	PG	0.04	2.64	73	1.36	62	0.52	3.34±0.95	0.62±0.07	3694	8253
1309+3531	PG	0.02	0.50	45	0.22	25	0.44	1.36±1.58	1.01±0.23	1723	4962
1351+640	PG	0.04	2.66	91	0.87	27	0.33	3.39±0.11	1.27±0.01	4699	3615
1351+6933	MARK279	0.03	6.68	101	4.64	96	0.67	5.28±0.36	1.18±0.05	6190	6556
1352+1820	PG	0.04	1.61	65	0.74	46	0.46	1.97±0.35	0.45±0.07	4351	3927
1411+442	PG	0.02	1.46	78	0.46	30	0.32	2.10±0.24	1.29±0.03	2373	2617
1415+2522	NGC5548	0.04	11.0	99	8.06	74	0.73	12.5±0.9	0.77±0.04	6259	6316
1415+4509	PG	0.02	1.04	74	0.48	70	0.46	1.03±0.33	-1.01±0.28	3404	6768
1416-129	PG	0.14	3.50	195	2.04	129	0.58	1.96±1.31	0.69±0.12	6125	6531
1426+0130	MARK1383	0.06	6.54	41	1.97	27	0.30	12.5±0.9	0.32±0.02	4091	5707
1440+3539	MARK478	0.02	4.50	82	0.81	23	0.18	5.33±0.34	0.43±0.05	2705	2913
1501+1037	MARK841	0.04	6.30	85	3.48	48	0.55	6.89±0.58	0.70±0.03	4216	4673
1512+370	B2	0.03	1.05	58	0.67	66	0.64	1.57±0.09	0.43±0.02	4858	8333
1534+5804	MARK290	0.03	4.39	81	2.52	74	0.55	4.31±0.54	0.69±0.04	4281	4987
1538+477 <sup>2</sup>	PG	0.03	1.45	141	0.60	66	0.41	0.68 ± ...	1.01±0.15	5875	6195
1556+2725	E	0.08	1.94	278	1.38	286	0.71	1.20±0.55	0.92±0.60	3746	7152
1613+6550	MARK876	0.06	3.04	81	1.85	68	0.61	4.35±0.38	0.74±0.03	6758	8043
1634+076 <sup>2</sup>	PG	0.11	3.80	63	1.06	29	0.28	5.32 ± ...	1.04±0.14	3738	4924
1704+608	3C351	0.05	0.76	42	0.31	24	0.40	1.92±1.54	0.20±0.03	3544	5363
1720+3055	MARK506	0.06	3.71	102	2.33	97	0.63	3.26±0.78	0.36±0.06	4558	5092
1721+3420	B2	0.06	4.17	109	3.35	148	0.80	4.26±1.94	0.65±0.26	4208	6678
1803+6737	KAZ102	0.09	3.91	129	1.89	88	0.48	3.20±0.36	0.80±0.11	4750	5972
1821+6419 <sup>1</sup>	KUV, H	0.03	7.22	150	3.83	100	0.53	5.66 ± ...	1.33±0.09	4038	4203
1833+3239	3C382.0	0.16	6.26	105	6.18	149	0.99	6.38±0.47	0.94±0.06	13331	14694
1845+7943	3C390.3	0.08	2.32	178	1.34	148	0.58	1.09±0.29	1.01±0.07	3793	8190
1916-5845	ESO141-G55	0.10	10.6	87	7.25	85	0.68	13.5±1.1	0.68±0.03	5238	6021
2041-1054	MARK509	0.08	19.5	126	11.4	104	0.58	16.2 ± 1.5	0.88±0.03	5933	5454
2130+0955	II ZW 136	0.09	5.56	82	2.10	61	0.38	5.21±1.21	1.15±0.05	2727	4277
2135-1446	PKS	0.09	1.53	133	0.95	86	0.62	1.60±0.39	1.18±0.14	8408	9192
2209+184	PG	0.10	2.29	142	1.23	96	0.54	2.91±1.27	0.96±0.11	7702	6595
2300+0836	NGC7469	0.10	12.9	100	8.43	84	1.01	15.6±1.22	0.88±0.03	3208	4324
2308+098	4C09.72	0.08	1.19	37	0.57	37	0.48	3.02±0.38	0.09±0.18	4195	5328
2316-0001	NGC7603	0.08	1.74	177	1.32	173	0.76	1.43±0.98	1.12±0.17	5511	6254

<sup>a</sup>in unit of  $10^{-13}$  erg cm<sup>-2</sup> s<sup>-1</sup>

<sup>b</sup>in unit of  $10^{-12}$  erg cm<sup>-2</sup> s<sup>-1</sup>

<sup>c</sup>in km s<sup>-1</sup>

REFERENCES.—(1) Laor et al. 1994; (2) Laor et al. 1995

TABLE 2  
X-RAY PARAMETERS

COORD	Z	$M_{abs}$	$N_H$ $10^{20} \text{ cm}^{-2}$	$\nu f_\nu$ (1keV) $10^{-12} \text{ erg cm}^{-2} \text{ s}^{-1}$	$\alpha_x$	ref	$\alpha_{uvx}$
0003+1955	0.025	-21.7	3.73±0.17	10.7±0.2	1.96±0.04	a	1.55
0007+1041	0.090	-22.7	7.85±0.52	2.78±0.41	1.00±0.17	a	1.55
0026+1259	0.142	-24.0	5.41±1.22	3.12±0.22	1.31±0.30	a	1.53
0050+1225	0.061	-23.4	6.90±0.72	5.63±0.24	2.05±0.12	a	1.39
0052+2509	0.155	-24.5	3.81±0.50	3.76±0.15	1.27±0.12	a	1.55
0119-2836	0.117	-23.9	1.45±0.25	4.58±0.19	1.69±0.11	b	1.48
0121-5903	0.046	-23.0	2.84±0.16	18.1±0.3	1.42±0.05	b	1.61
0124+1855	0.017	-20.2	4.69±0.68	5.60±0.27	1.31±0.15	b	1.38
0157+0009	0.163	-23.9	2.72±0.91	0.67±0.07	1.85±0.17	a	1.79
0203-0031	0.043	-21.3	2.71±0.75	1.29±0.08	1.12±0.25	b	1.58
0205+0228	0.155	-24.2	3.46±0.36	1.84±0.07	2.30±0.09	b	1.58
0232-0900	0.043	-22.4	3.10±1.60	17.4± 7.9	1.68±0.40	b	1.24
0236-5224	0.045	-22.8	3.15±0.24	15.2±0.3	1.37±0.06	b	1.03
0405-123	0.574	-27.7	3.27±0.63	2.94±0.16	1.19±0.17	b	1.52
0430+0514	0.033	-20.8	16.6±0.8	26.9±9.5	1.15±0.33	b	1.22
0513-0012	0.033	-22.2	10.4±0.4	14.6±0.2	1.61±0.06	b	1.67
0637-752	0.656	-27.0	11.1±3.1	2.18±1.82	1.45±0.84	b	1.53
0702+6440	0.079	-23.1	4.16±1.04	2.85±0.22	1.38±0.24	b	1.65
0738+4945	0.022	-20.9	9.30±1.70	41.4±8.5	1.90±0.24	b	1.15
0743+6103	0.030	-21.1	4.05±0.51	5.98±0.23	1.31±0.12	b	1.30
0821+7611	0.100	-23.8	3.65±0.58	6.21±0.29	1.58±0.15	b	1.55
0844+3456	0.064	-23.9	4.15±2.71	0.32±0.06	1.63±0.65	a	2.08
0915+1630	0.029	-21.4	3.5±1.8	17.0±7.6	1.57±0.40	b	1.01
0921+5230	0.036	-20.6	1.37±0.09	17.8±0.2	1.40±0.04	a	1.05
0923+129	0.029	-21.0	3.51±0.47	7.20±0.26	1.27±0.14	a	1.34
0953+415	0.239	-25.6	1.47±0.36	1.53±0.09	1.71±0.16	a	1.55
0955+326	0.533	-26.7	3.34±4.12	0.16±0.04	1.60±1.29	a	2.22
1012+008	0.185	-24.4	3.54±...	1.28±...	1.66±...	a	1.48
1028+3118	0.177	-23.1	5.92±...	0.65±...	1.98±...	c	1.70
1100+772	0.313	-25.8	3.45±1.69	1.74±0.27	1.64±0.68	a	1.59
1103+7250	0.009	-20.5	2.73±0.12	24.8±0.3	1.15±0.04	b	0.99
1114+445	0.144	-23.7	1.50±1.20	0.34±0.05	1.36±0.49	a	1.80
1116+2135	0.177	-25.2	1.44±0.20	2.18±0.06	1.68±0.06	a	1.69
1119+1200	0.049	-22.0	2.64±...	2.40±...	1.98±...	a	1.52
1202+2810	0.165	-24.4	1.87±0.28	1.50±0.05	1.28±0.11	a	1.44
1211+1419	0.085	-23.9	3.25±0.60	4.93±0.32	2.13±0.16	a	1.60
1216+069	0.334	-25.9	2.03±0.60	1.57±0.11	1.54±0.24	a	1.46
1226+0219	0.158	-26.9	1.39±0.19	34.9±0.9	1.07±0.08	a	1.47
1229+2026	0.064	-22.4	1.81±0.20	3.65±0.10	1.64±0.08	a	1.57
1237-0504	0.009	-19.7	2.02±0.61	6.77±0.42	1.08±0.22	b	1.26
1244+0240	0.048	-26.2	6.23±0.51	1.26±0.38	0.77±0.24	a	1.48
1307+0835	0.155	-24.6	2.21±0.45	1.73±0.09	1.64±0.16	a	1.63
1309+3531	0.184	-24.7	0.41±0.71	0.50±0.08	1.29±0.37	a	1.70
1351+640	0.088	-24.1	2.54±1.80	0.36±0.06	1.53±0.63	a	1.97
1351+6933	0.031	-21.2	1.80±0.5	128.± 21.	1.15±0.17	b	0.81
1352+1820	0.152	-24.0	1.89±0.55	1.51±0.09	1.64±0.17	a	1.55
1411+442	0.090	-23.7	1.10±1.00	0.058±0.011	1.97±0.46	a	2.26
1415+2522	0.017	-20.7	1.43±0.23	24.5±0.80	1.30±0.10	b	1.35
1415+4509	0.114	-23.5	0.72±0.42	0.55±0.06	1.62±0.21	a	1.63
1416-129	0.129	-24.1	7.21±0.31	3.92±0.54	1.19±0.16	a	1.34
1426+0130	0.086	-23.4	2.80±0.32	6.24±0.19	1.55±0.09	a	1.64
1440+3539	0.077	-23.4	1.38±0.38	3.15±0.30	2.32±0.20	a	1.60
1501+1037	0.036	-22.2	2.34±0.27	10.0±0.3	1.56±0.12	a	1.41
1512+370	0.371	-25.6	1.14±0.56	9.82±0.08	1.16±0.24	a	1.10
1534+5804	0.030	-20.7	2.07±0.56	3.23±0.18	1.17±0.21	a	1.55
1538+477	0.770	-27.5	...	0.20±...	1.50±...	c	1.75
1556+2725	0.090	-21.8	3.50±2.10	1.90±0.40	1.05±0.21	b	1.33
1613+6550	0.129	-23.5	2.17±0.52	3.57±0.22	1.38±0.20	a	1.53
1634+706	1.335	-30.1	4.42±1.57	0.40±0.04	1.38±0.46	a	2.04
1704+608	0.371	-26.5	2.54±1.21	0.48±0.05	1.30±0.41	a	1.79
1720+3055	0.043	-21.7	2.31±0.97	2.38±0.22	0.91±0.33	b	1.56
1721+3420	0.206	-24.0	2.9± 1.0	45.6±11.1	1.27±0.25	b	0.99
1803+6737	0.136	-23.6	4.44±1.27	1.65±0.14	1.39±0.31	b	0.86
1821+6419	0.297	-27.1	3.05±1.52	3.89±0.36	1.17±0.49	b	1.57
1833+3239	0.059	-21.3	8.6 ±1.7	125.±...	1.39±0.24	c	0.86
1845+7943	0.057	-21.6	5.90±0.56	12.1±0.76	0.86±0.14	b	0.98
1916-5845	0.037	-22.9	5.46±0.37	14.9±0.4	1.37±0.07	b	1.47
2041-1054	0.035	-23.3	3.88±0.41	25.8±0.8	1.58±0.10	b	1.39
2130+0955	0.063	-23.6	4.65±...	0.68±...	2.25±...	a	1.93
2135-1446	0.200	-24.8	3.12±1.35	2.46±0.27	0.82±0.39	b	1.40
2209+184	0.070	-22.3	4.89±...	9.04±...	1.20±...	a	1.25
2300+0836	0.017	-21.6	5.68±0.27	18.2±0.3	1.38±0.05	b	1.46
2308+098	0.432	-26.0	4.07±1.30	1.06±0.10	1.44±0.34	a	1.71
2316-0001	0.029	-21.5	4.25±0.63	3.78±0.17	1.03±0.17	b	1.28

REFERENCES.— (a) Wang, Brinkmann & Bergeron 1996; (b) this paper; (c) Brinkmann et al. 1995

TABLE 3  
CORRELATION MATRIX

		$\alpha_{sx}$	$\alpha_{uvx}$	$\alpha_{uv}$	$\alpha_{\epsilon uv}$	$M_{abs}$	EW Ly $\alpha$	EW CIV	$\frac{CIV}{Ly\alpha}$	FWHM Ly $\alpha$	FWHM CIV
$\alpha_{sx}$	$R_s$	1.00	0.42	-0.22	-0.09	-0.15	-0.20	-0.46	-0.43	-0.22	-0.21
...	$P_r$	0.00	$2 \times 10^{-4}$	0.06	0.46	0.22	0.09	$5 \times 10^{-5}$	$1 \times 10^{-4}$	0.05	0.07
$\alpha_{uvx}$	$R_s$	0.42	1.00	-0.16	0.83	-0.50	-0.43	-0.59	-0.58	-0.28	-0.20
...	$P_r$	$2 \times 10^{-4}$	0.00	0.17	$8 \times 10^{-19}$	$5 \times 10^{-6}$	$2 \times 10^{-4}$	$3 \times 10^{-8}$	$6 \times 10^{-8}$	0.02	0.08
$\alpha_{uv}$	$R_s$	-0.22	-0.16	1.00	-0.04	0.13	0.38	0.09	-0.05	-0.09	-0.30
...	$P_r$	0.06	0.17	0.00	0.71	0.28	$1 \times 10^{-3}$	0.47	0.65	0.47	$8 \times 10^{-3}$
$\alpha_{\epsilon uv}$	$R_s$	-0.09	0.83	-0.04	1.00	-0.50	-0.30	-0.37	-0.35	-0.16	-0.10
...	$P_r$	0.46	$8 \times 10^{-19}$	0.71	0.00	$5 \times 10^{-6}$	0.01	$1 \times 10^{-3}$	$2 \times 10^{-3}$	0.17	0.38
$M_{abs}$	$R_s$	-0.15	-0.50	0.13	-0.50	1.00	0.17	0.33	0.30	0.18	0.04
...	$P_r$	0.22	$5 \times 10^{-6}$	0.28	$5 \times 10^{-6}$	0.00	0.14	$4 \times 10^{-3}$	0.01	0.11	0.75
EW	$R_s$	-0.20	-0.43	0.38	-0.30	0.17	1.00	0.68	0.35	0.36	0.24
Ly $\alpha$	$P_r$	0.09	$2 \times 10^{-4}$	$1 \times 10^{-3}$	0.01	0.14	0.00	$4 \times 10^{-11}$	$3 \times 10^{-3}$	$2 \times 10^{-3}$	0.04
EW	$R_s$	-0.46	-0.59	0.09	-0.37	0.33	0.68	1.00	0.72	0.41	0.44
CIV	$P_r$	$5 \times 10^{-5}$	$3 \times 10^{-8}$	0.47	$1 \times 10^{-3}$	$4 \times 10^{-3}$	$4 \times 10^{-11}$	0.00	$3 \times 10^{-13}$	$2 \times 10^{-4}$	$1 \times 10^{-4}$
$\frac{CIV}{Ly\alpha}$	$R_s$	-0.43	-0.58	-0.05	-0.35	0.30	0.35	0.72	1.00	0.30	0.38
...	$P_r$	$1 \times 10^{-4}$	$6 \times 10^{-8}$	0.65	$2 \times 10^{-3}$	$1 \times 10^{-3}$	$3 \times 10^{-3}$	$3 \times 10^{-13}$	0.00	0.01	$1 \times 10^{-3}$
FWHM	$R_s$	-0.23	-0.28	-0.09	-0.16	0.19	0.36	0.42	0.30	1.00	0.62
Ly $\alpha$	$P_r$	0.05	0.02	0.47	0.17	0.11	$2 \times 10^{-3}$	$2 \times 10^{-4}$	0.01	0.00	$5 \times 10^{-9}$
FWHM	$R_s$	-0.21	-0.20	-0.30	-0.10	0.04	0.24	0.44	0.38	0.62	1.00
CIV	$P_r$	0.07	0.08	0.08	0.38	0.75	0.04	$1 \times 10^{-4}$	$1 \times 10^{-3}$	$5 \times 10^{-9}$	0.00